

## The process of phase formation in the synthesis of $\text{Al}_2\text{O}_3$ - $\text{Y}_2\text{O}_3$ - $\text{SiO}_2$ frit by sol-gel and coprecipitation method

Tran Van Cuong<sup>1\*</sup>, Ninh Duc Ha<sup>1</sup>, Dang Quoc Khanh<sup>2</sup>, Nguyen Van Canh<sup>1</sup>,  
Ho Ngoc Minh<sup>1</sup>, Trieu Khuong<sup>1</sup>, Nguyen Thi Hoa<sup>1</sup>, Ngo Van Hoanh<sup>1</sup>, Le Trung Hieu<sup>1</sup>

<sup>1</sup>Institute of Materials, Biology and Environment, Academy of Military Science and Technology, 17 Hoang Sam, Nghia Do, Cau Giay, Ha Noi, Vietnam;

<sup>2</sup>HaNoi University of Science and Technology, 1 Dai Co Viet, Hai Ba Trung, Hanoi, Vietnam.

\*Corresponding author: trancuong.hhv1@gmail.com

Received 28 Feb. 2025; Revised 25 Apr. 2025; Accepted 10 Jun. 2025; Published 25 Jun. 2025.

DOI: <https://doi.org/10.54939/1859-1043.j.mst.104.2025.94-102>

### ABSTRACT

*Frits are utilized in various high-temperature and structural applications due to their exceptional properties. However, most frits are fabricated via solid-state reactions, which require high sintering temperatures and extended time to achieve homogeneity. Therefore, this study investigates the phase transition in the  $\text{Al}_2\text{O}_3$  -  $\text{Y}_2\text{O}_3$  -  $\text{SiO}_2$  frit using sol-gel method, which enables lower synthesis temperature and achieves higher purity. The energy dispersive X-ray spectroscopy (EDX) results confirm the successful fabrication of  $\text{Al}_2\text{O}_3$  -  $\text{Y}_2\text{O}_3$  -  $\text{SiO}_2$  frits. The effect of the sintering conditions on the phase transition was studied. The X-ray diffraction patterns revealed that the frit remained completely amorphous up to 1000 °C. Although the crystalline phases  $\text{Y}_2\text{O}_3 \cdot 2\text{SiO}_2$ ,  $\text{Y}_2\text{O}_3 \cdot \text{SiO}_2$ , and  $\alpha\text{-Al}_2\text{O}_3$  begin to appear around 1100 °C, the overall degree of crystallinity increases with temperature, indicating a gradual transformation from an amorphous to a more crystalline structure. A fully crystallized structure of the  $\text{Al}_2\text{O}_3$  -  $\text{Y}_2\text{O}_3$  -  $\text{SiO}_2$  frit is observed at 1400 °C. The differential thermal analysis (TGA) results confirm the glass transition, crystallization and eutectic temperature of the  $\text{Al}_2\text{O}_3$  -  $\text{Y}_2\text{O}_3$  -  $\text{SiO}_2$  frit. The optimized sintering condition was determined to be 1400 °C for 5 hours.*

**Keywords:**  $\text{Y}_2\text{O}_3$  -  $\text{Al}_2\text{O}_3$  -  $\text{SiO}_2$ ; Frit; Ceramics; SiAlON.

### 1. INTRODUCTION

The Yttria-Alumina-Silica ( $\text{Al}_2\text{O}_3$  -  $\text{Y}_2\text{O}_3$  -  $\text{SiO}_2$ ) ternary oxide system is widely used in high-performance applications. It plays a key role in the development of materials such as glass-ceramics, refractories, sintering additives, and SiAlON ceramics [1]. Among these, SiAlON ceramics stand out as some of the most advanced materials used in industry today. These ceramics demonstrate outstanding resistance to corrosion in molten metal environments, leading to an extended service life of approximately 12 to 18 months. As a result, SiAlON-based materials are favored for extreme working conditions involving high temperatures and aggressive molten metals [2].

Due to high production costs, SiAlON ceramics are manufactured by only a few companies, predominantly in Japan, the United States, the United Kingdom, and China.. Japan leads global production with a 60% share, followed by the US at 30%, while Europe and China each contribute about 5% [3]. Despite their advantages, the high cost limits widespread adoption, prompting the use of less efficient, more economical alternatives.

A noteworthy component of SiAlON ceramic is the use of 1A6Y3S frit ( $\text{Al}_2\text{O}_3$  -  $\text{Y}_2\text{O}_3$  -  $\text{SiO}_2$ ) as an effective sintering additive [4]. This additive reduces sintering temperatures while enhancing the mechanical properties of the ceramics. Various synthesis methods have been used for producing 1A6Y3S frit, including sol-gel Pechini, sol-gel, co-precipitation, hydrothermal techniques, combustion combined with microwave processing, peptization of oxalate gels, acid acetate-based gels, and melting routes [5]. Among these, the melting method remains prevalent

due to its practicality for large-scale production. Typically,  $Y_2O_3$ ,  $Al_2O_3$ , and  $SiO_2$  oxides are employed as precursors.

Although sol-gel and co-precipitation techniques are well established in material science, their application to the synthesis of advanced ceramic additives remains limited. These methods offer several advantages: lower synthesis temperatures (typically below  $1000\text{ }^\circ\text{C}$ ), precise control of phase composition, nanoscale homogeneity, and tailored particle size distribution [6–10].

This study investigates the combination of sol-gel and co-precipitation approaches to produce a homogeneous oxide mixture. Melting and rapid quenching in water were subsequently applied to enhance uniformity and reduce the melting temperature of the 1A6Y3S frit. Additionally, the effects of synthesis conditions on the structural and physical properties of the frit are systematically analyzed.

## 2. EXPERIMENTAL

### 2.1. Synthesis process of $Al_2O_3$ - $Y_2O_3$ - $SiO_2$ frits

The  $SiO_2$  precursor was prepared via the sol-gel method. Initially, an aqueous  $Na_2SiO_3$  solution was stirred continuously and heated to  $80\text{ }^\circ\text{C}$ . A  $0.5\text{ M}$   $HCl$  solution was then added dropwise under constant stirring until the pH reached 9–10. Continuous agitation throughout the acid addition ensured homogeneity in gel formation. The resulting gel was dried at  $90\text{ }^\circ\text{C}$  until complete solvent evaporation occurred. The dried material was subsequently washed multiple times with ethanol and deionized water to remove soluble by-products and then ground to yield fine  $SiO_2$  powder.

The  $Al_2O_3$  and  $Y_2O_3$  powders were synthesized via a coprecipitation technique. Equimolar ( $1\text{ M}$ ) aqueous solutions of  $Al(NO_3)_3 \cdot 9H_2O$  and  $Y(NO_3)_3 \cdot 6H_2O$  were prepared and thoroughly mixed. Aqueous ammonia was added dropwise as the precipitating agent until the solution pH stabilized between 8.1 and 8.3. The resulting suspension was aged under mild agitation at  $80\text{ }^\circ\text{C}$  for 30 minutes to allow complete precipitation and maturation of the hydroxide phases. The precipitates were then collected via vacuum filtration, washed repeatedly with ethanol and deionized water to remove residual ions, and dried at  $100\text{ }^\circ\text{C}$ . The dried powders were manually ground using an agate mortar and subsequently calcined at an appropriate temperature to convert the hydroxides into their respective oxide forms.

The obtained  $Al_2O_3$ ,  $Y_2O_3$ , and  $SiO_2$  powders were weighed according to predetermined molar ratios (table 1) and dispersed in isopropanol. The resulting suspension was subjected to planetary ball milling for 30 minutes to ensure fine and homogeneous mixing. The mixture was then dried at  $\sim 100\text{ }^\circ\text{C}$  to remove the solvent. The dry powder blend was transferred to a platinum crucible and placed within an alumina ceramic support boat, then introduced into a high-temperature furnace for melting. Melting was conducted at  $1000\text{ }^\circ\text{C}$ ,  $1100\text{ }^\circ\text{C}$ ,  $1200\text{ }^\circ\text{C}$ ,  $1300\text{ }^\circ\text{C}$ , and  $1400\text{ }^\circ\text{C}$  with a controlled heating rate of  $10\text{ }^\circ\text{C min}^{-1}$ . Upon reaching the target temperature, the samples were rapidly quenched in water to obtain glassy frit fragments. These fragments, typically several millimeters in size, were milled in ethanol using a planetary ball mill until a particle size of less than  $5\text{ }\mu\text{m}$  was achieved.

**Table 1.** Composition of 1A6Y3S frit in terms of oxides and corresponding melting temperature.

No	Name	Sample	Composition, wt%			Method
			$Al_2O_3$	$Y_2O_3$	$SiO_2$	
1	O	1A6Y3S	10.8	60.5	28.7	Sol-gel
2	O'	1A6Y3S_M	10.8	60.5	28.7	Mixed oxides

### 2.2. Materials characterization

The thermal properties of the 1A6Y3S frit, including the glass transition temperature ( $T_g$ ) and the crystallization peak temperature ( $T_c$ ), were determined using Differential Thermal Analysis (DTA) performed on a Linseis STA PT 2400 thermal analyzer (Germany). Phase identification and crystallographic structure were analyzed by X-ray Powder Diffraction (XRD) using a Bruker diffractometer (Germany).

The morphological characteristics of the 1A6Y3S particles were examined by Scanning Electron Microscopy (SEM) utilizing a HITACHI S-4800 microscope (Japan). Hardness measurements were carried out using a ZwickRoell hardness testing machine (Germany). For each sample, five indentations were made under a load of 50 g applied for 10 seconds, and the average value was reported as the representative hardness. The bulk density and porosity of the samples were measured using a helium gas pycnometer (AccuPyc II 1340, Micromeritics, USA), following the standard procedure outlined in TCVN 6530-3:2016. For each specimen, ten independent measurements were conducted, and the average was taken as the final reported value.

### 3. RESULTS AND DISCUSSION

#### 3.1. Investigation of the phase transition temperature and crystallization temperature of the $\text{Al}_2\text{O}_3 - \text{Y}_2\text{O}_3 - \text{SiO}_2$

The phase transition temperature and crystallization temperature of the 1A6Y3S frit ( $\text{Al}_2\text{O}_3 - \text{Y}_2\text{O}_3 - \text{SiO}_2$ ) were investigated using differential thermal analysis (DTA). The results are presented in figure 1 and table 2.

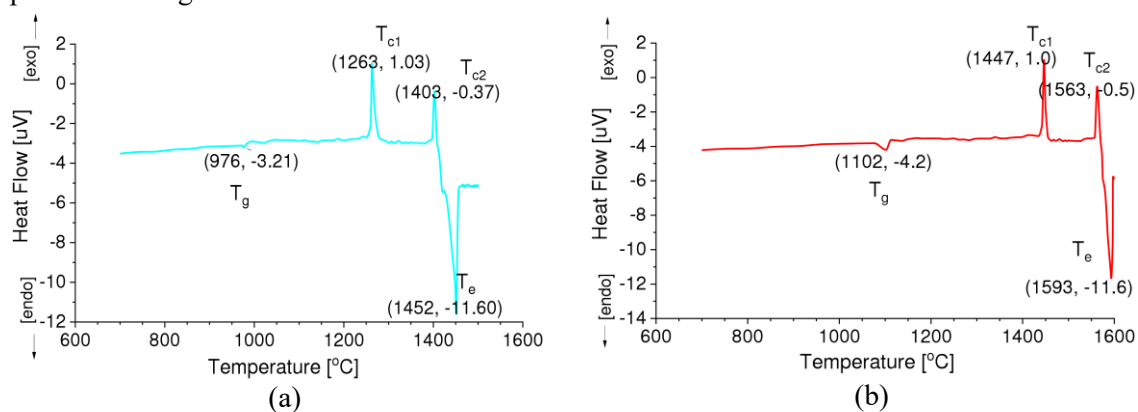


**Figure 1.** Differential Thermal Analysis (DTA) of the synthesized 1A6Y3S frits from: (a) Sol-gel; (b) Mixed oxides.

**Table 2.** DTA analysis results of 1A6Y3S frit.

No	Sample	$T_g$ (°C)	$T_{C1}$ (°C)	$T_{C2}$ (°C)	$T_e$ (°C)
1	1A6Y3S	976	1263	1403	1452
2	1A6Y3S_M	1102	1447	1563	1593

The glass transition temperature  $T_g$  of the 1A6Y3S sample was determined to be 976 °C. A marked melting behavior was observed in the temperature range of approximately 1300–1400 °C. Differential thermal analysis revealed two distinct crystallization peaks, with the first ( $T_{c1}$ ) occurring at 1263 °C and the second ( $T_{c2}$ ) at approximately 1403 °C. Additionally, a eutectic reaction was detected at about 1452 °C.

When compared with the 1A6Y3S\_M sample synthesized via the conventional oxide-mixing method, the sol-gel/co-precipitation-derived 1A6Y3S sample exhibited lower characteristic temperatures ( $T_g$ ,  $T_{c1}$ ,  $T_{c2}$ ,  $T_e$ ). This reduction in thermal transition points can be attributed to the nature of the raw materials and synthesis process. Specifically, the sol-gel and co-precipitation

techniques produced amorphous oxides with a highly homogeneous microstructure and nanoscale particle sizes. Such structural characteristics enhance reactivity and reduce the thermal stability of the glass network, leading to lower melting and crystallization temperatures compared to the oxide-mixed sample, which contained larger and more crystalline precursor particles.

### 3.2. Effect of melting temperature on the phase composition of the $\text{Al}_2\text{O}_3$ - $\text{Y}_2\text{O}_3$ - $\text{SiO}_2$

To investigate the influence of melting temperature on the phase composition of the 1A6Y3S frit, oxide mixtures were subjected to heat treatment at 1000 °C, 1100 °C, 1200 °C, 1300 °C, and 1400 °C for 0.5 hours. The resulting frits were rapidly quenched and subsequently analyzed to determine their phase constitution. X-ray diffraction (XRD) analysis was employed to identify crystalline phases present in the samples and to evaluate the evolution of crystallinity as a function of temperature.

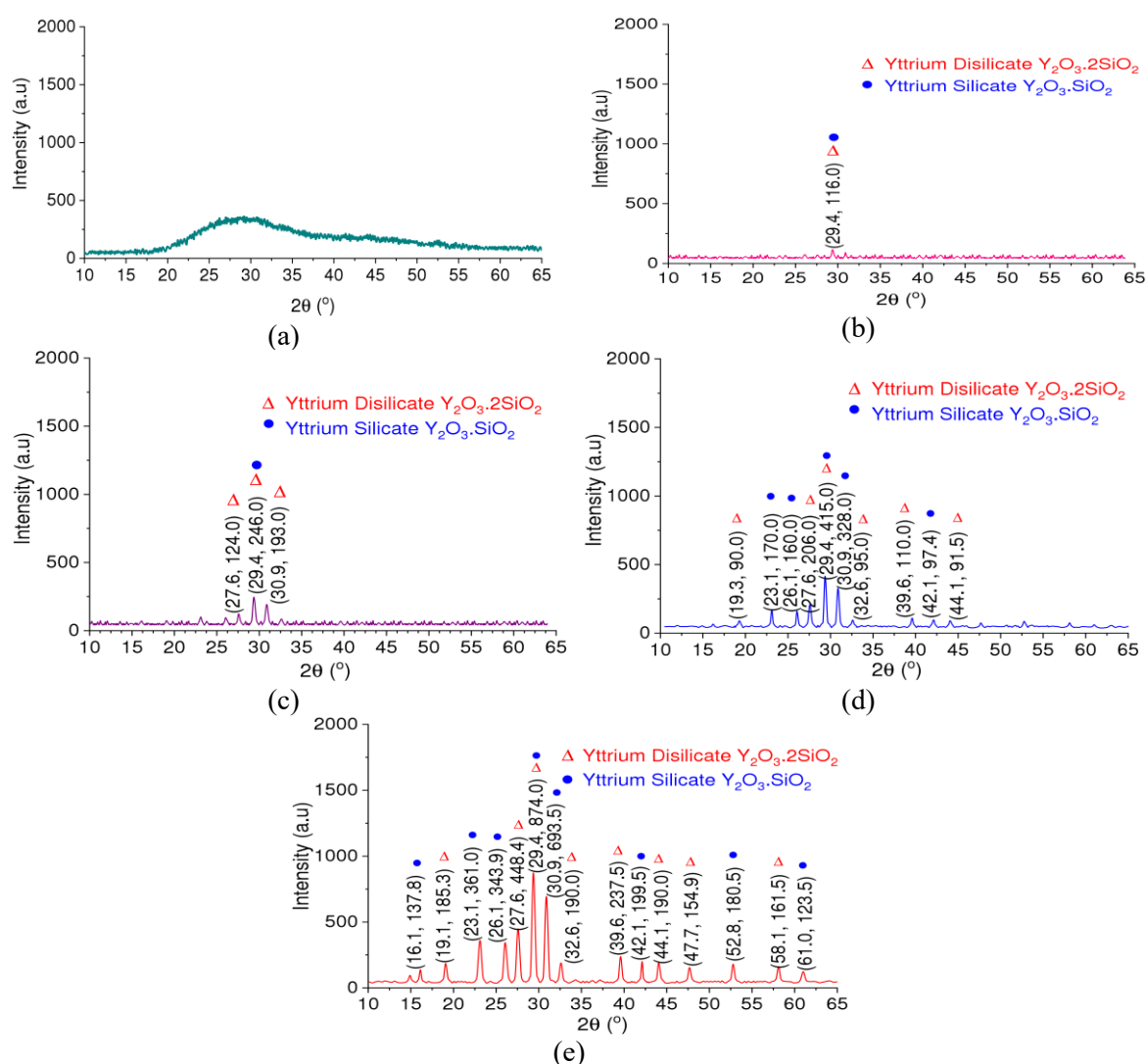


**Figure 2.** XRD patterns of 1A6Y3S frit fired for 0.5 hours at (a) 1000 °C, (b) 1100 °C, (c) 1200 °C, (d) 1300 °C, and (e) 1400 °C.

As illustrated in figure 2, X-ray diffraction (XRD) analysis revealed no discernible diffraction peaks at temperatures below 1000 °C, confirming the retention of a fully amorphous structure

without crystalline phase formation. Initial crystallization of yttrium disilicate (YDS,  $\text{Y}_2\text{O}_3 \cdot 2\text{SiO}_2$ ) was observed at 1100 °C, evidenced by a low-intensity diffraction peak centered at  $2\theta = 29.4^\circ$ . Upon heating to 1200 °C, the YDS phase exhibited enhanced crystallinity, as indicated by a pronounced increase in peak intensity at  $2\theta = 29.4^\circ$ , accompanied by the emergence of a secondary weak peak at  $2\theta = 27.4^\circ$ . Concurrently, the yttrium silicate (YS,  $\text{Y}_2\text{O}_3 \cdot \text{SiO}_2$ ) phase began to nucleate, marked by two low-intensity peaks at  $2\theta = 29.4^\circ$  and  $30.9^\circ$ .

Progressive phase evolution was observed at 1300 °C. The YDS phase developed additional diffraction features at  $2\theta = 19.3^\circ$ ,  $32.6^\circ$ ,  $39.6^\circ$  and  $44.1^\circ$ . Furthermore, the intensities of existing YDS peaks at  $2\theta = 27.6^\circ$  and  $29.4^\circ$  increased significantly. The YS phase concurrently formed new peaks at  $2\theta = 23.1^\circ$ ,  $26.1^\circ$ , and  $42.1^\circ$ , while existing YS peaks at  $29.4^\circ$  and  $30.9^\circ$  intensified.

At 1400 °C, the YDS phase (JCPDS No. 21-1457 [11]) displayed further structural maturation, with new peaks emerging at  $2\theta = 47.7^\circ$  and  $58.1^\circ$ . Peak intensities across the YDS profile exhibited substantial enhancement:  $19.1^\circ$ ,  $27.6^\circ$ ,  $29.4^\circ$ ,  $32.6^\circ$ ,  $39.6^\circ$ ,  $44.1^\circ$ , and  $47.7^\circ$ . Similarly, the YS phase (JCPDS No. 21-1458 [12]) demonstrated progressive crystallization, manifesting new peaks at  $2\theta = 16.1^\circ$ ,  $52.8^\circ$ , and  $61.0^\circ$ , alongside intensified peaks at  $23.1^\circ$ ,  $26.1^\circ$ ,  $29.4^\circ$ ,  $30.9^\circ$ , and  $42.1^\circ$ .

The sequential formation of crystalline phases followed the order  $\text{Y}_2\text{O}_3 \cdot 2\text{SiO}_2 \rightarrow \text{Y}_2\text{O}_3 \cdot \text{SiO}_2$ , consistent with the lower melting point of  $\text{SiO}_2$  (1710 °C [13]) relative to  $\text{Y}_2\text{O}_3$  (2425 °C [14]). The preferential formation of  $\text{Y}_2\text{O}_3 \cdot 2\text{SiO}_2$  is attributed to the higher  $\text{SiO}_2$  content, which acts as a fluxing agent, facilitating lower-temperature crystallization kinetics. Notably, peak intensities stabilized above 1300 °C, with maximum crystallinity achieved between 1300–1400 °C, corroborating differential thermal analysis (DTA) data. Consequently, 1400 °C was identified as the optimal synthesis temperature for the 1A6Y3S frit.

To evaluate melting temperature effects on phase composition, oxide mixtures were processed at 1500 °C and 1600 °C (denoted as 1A6Y3S\_M). Subsequent XRD analysis confirmed the retention of YDS and YS phases, with no observable polymorphic transitions or secondary phase formation.

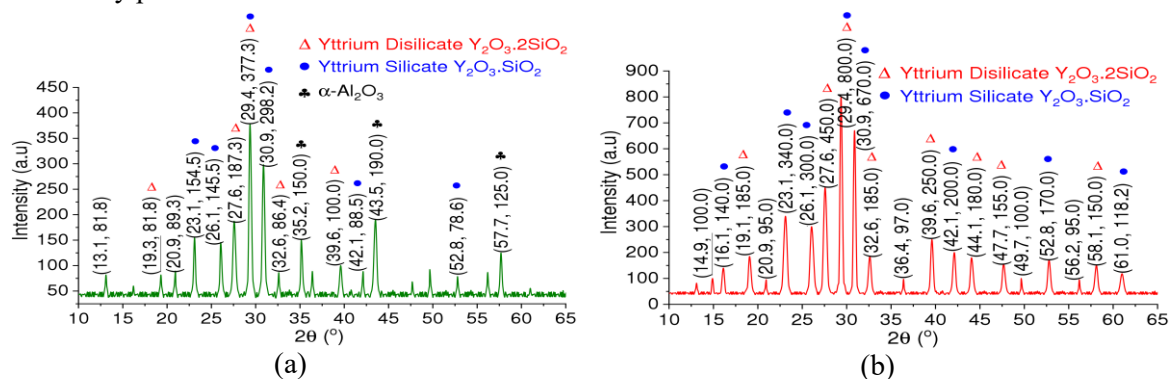


**Figure 3.** XRD patterns of 1A6Y3S\_M frit fired for 0.5 hours at: (a) 1500 °C, (b) 1600 °C.

As demonstrated in figure 3, frit 1A6Y3S\_M synthesized via conventional solid-state mixing of  $\text{Al}_2\text{O}_3$ ,  $\text{Y}_2\text{O}_3$  and  $\text{SiO}_2$  oxides exhibited a melting temperature approximately 200 °C higher than that of samples prepared via sol-gel synthesis. XRD analysis of the traditionally processed sample sintered at 1500 °C (0.5 h) revealed residual  $\alpha\text{-Al}_2\text{O}_3$  (JCPDS No. 46-1212), identified by diffraction peaks at  $2\theta = 35.2^\circ$ ,  $43.5^\circ$ , and  $57.7^\circ$  with weak intensities. Notably, this method exhibited inferior phase formation control compared to sol-gel synthesis, as evidenced by the emergence of non-indexed diffraction features at  $2\theta = 13.1^\circ$ ,  $20.9^\circ$ , and  $39.6^\circ$ .

Elevating the sintering temperature to 1600 °C (0.5 h) for the traditionally synthesized

1A6Y3S\_M resulted in the complete dissolution of  $\alpha$ -Al<sub>2</sub>O<sub>3</sub>, though the melting temperature disparity (~200 °C relative to sol-gel-derived samples) persisted. Despite the absence of  $\alpha$ -Al<sub>2</sub>O<sub>3</sub>, phase complexity remained unresolved, with unidentified peaks observed at  $2\theta = 14.9^\circ, 20.9^\circ, 36.4^\circ, 49.7^\circ,$  and  $56.2^\circ$ . These findings underscore the challenges associated with phase regulation in conventional solid-state synthesis, which contrasts sharply with the enhanced homogeneity and phase purity achieved via sol-gel methods.

### 3.3. Effect of melting time on the structure of 1A6Y3S frit

In addition to the melting temperature, the duration of the melting process significantly influences the structural characteristics of the material. To investigate the effect of melting time on phase composition, 1A6Y3S frit samples were subjected to thermal treatment at 1400 °C for periods of 5 and 10 hours. The resulting crystalline structures of the samples corresponding to each duration are presented in figure 4.

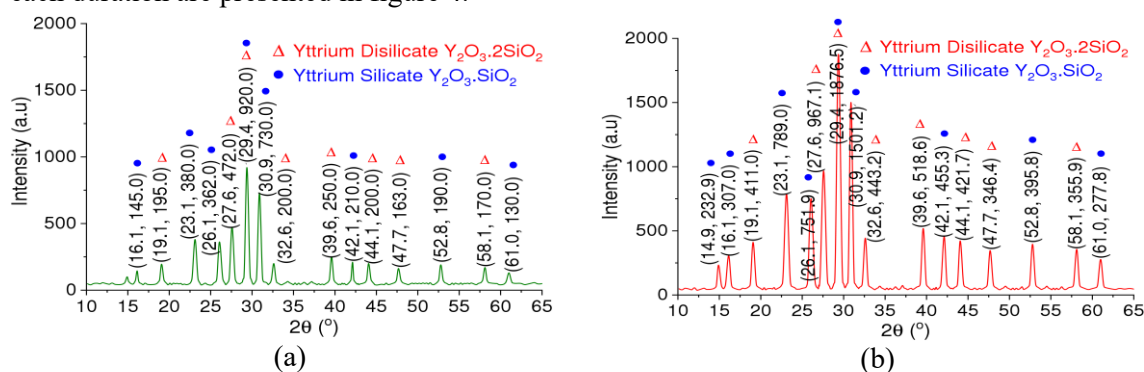


Figure 4. XRD patterns of the 1A6Y3S frit melted at 1400 °C for (a) 5 h and (b) 10 h.

Upon melting at 1400 °C for 10 hours, the peak intensities associated with the Yttrium Disilicate ( $Y_2O_3 \cdot 2SiO_2$ ) crystalline phase (JCPDS No. 21-1457) at  $2\theta$  values of  $19.1^\circ, 27.6^\circ, 29.4^\circ, 32.6^\circ, 39.6^\circ, 44.1^\circ, 47.7^\circ,$  and  $58.1^\circ$ .

Simultaneously, the formation of the Yttrium Silicate ( $Y_2O_3 \cdot SiO_2$ ) phase (JCPDS No. 21-1458) progressed, as evidenced by the appearance of a new diffraction peak at  $2\theta = 14.9^\circ$ . Furthermore, the intensities of existing peaks at  $2\theta = 16.1^\circ, 23.1^\circ, 26.1^\circ, 29.4^\circ, 30.9^\circ, 42.1^\circ, 52.8^\circ,$  and  $61.0^\circ$  were enhanced.

X-ray diffraction (XRD) analysis clearly indicates that the peak intensities corresponding to both Yttrium Disilicate ( $Y_2O_3 \cdot 2SiO_2$ ) and Yttrium Silicate ( $Y_2O_3 \cdot SiO_2$ ) phases are significantly higher in the sample subjected to a 10-hour melting duration compared to the sample melted for 5 hours. This suggests an enhancement in crystallinity with prolonged melting time.

Additionally, morphological changes in the 1A6Y3S samples as a function of melting duration (0.5, 5, and 10 hours) were examined using Scanning Electron Microscopy (SEM), as shown in figure 5.

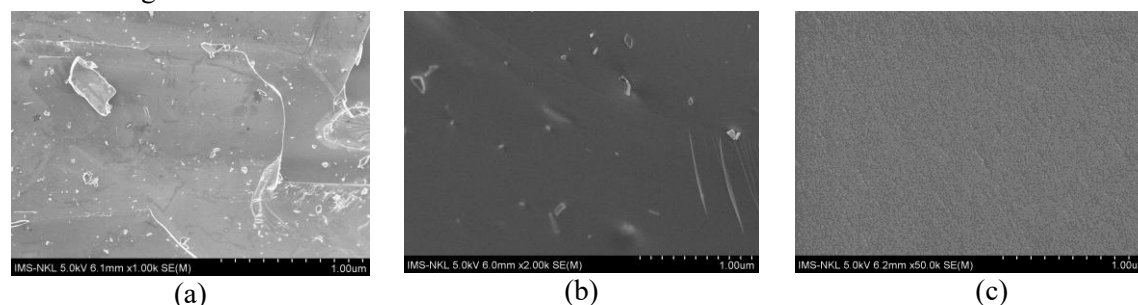
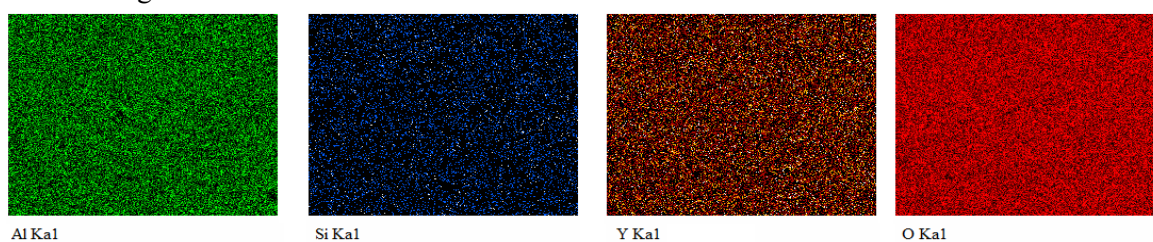


Figure 5. SEM image of 1A6Y3S frit melted at 1400 °C for 0.5 (a), 5 (b) and 10 hours (c).

The results indicate that the 1A6Y3S sample melted at 1400 °C for 10 hours exhibits a higher degree of crystallization and a more uniform distribution of crystalline phases compared to samples treated for 0.5 and 5 hours. A fine particle microstructure was observed in both the 5-hour and 10-hour samples, which is consistent with the increased crystallinity. This refined microstructure is believed to contribute to the emergence of secondary crystallization peaks observed in the Differential Thermal Analysis (DTA) of the 1A6Y3S frit.

The combined interpretation of Scanning Electron Microscopy (SEM) images and X-ray Diffraction (XRD) patterns confirms that the crystalline structure of the sample primarily consists of Yttrium Disilicate ( $Y_2O_3 \cdot 2SiO_2$ ) and Yttrium Silicate ( $Y_2O_3 \cdot SiO_2$ ) phases. Furthermore, the elemental composition and spatial distribution within the 1A6Y3S frit subjected to a 5-hour melting duration were analyzed using Energy-Dispersive X-ray (EDX) Mapping, as shown in figure 6.



**Figure 6.** EDX Mapping of the frits melted for 5 hours: 1A6Y3S at 1400 °C.

EDX mapping analysis of the 1A6Y3S frit melted at 1400 °C for 5 hours revealed a homogeneous distribution of the constituent elements Al, Si, Y, and O throughout the sample.

Furthermore, comparative analysis of the XRD patterns and SEM micrographs indicated minimal structural differences between the samples held at 1400 °C for 5 and 10 hours. Based on the combined results from XRD, SEM, and EDX mapping, a holding time of 5 hours was determined to be optimal, providing sufficient crystallinity and elemental homogeneity without necessitating extended thermal treatment.

### 3.4. Physical and thermal properties of 1A6Y3S and 1A6Y3S\_M frits

1A6Y3S and 1A6Y3S\_M frits were studied using different quantitative tools to determine their physical properties such as density, hardness and porosity.

**Table 3.** Mechanical and physical properties of 1A6Y3S and 1A6Y3S\_M frits.

No	Sample	Mechanical properties: Hardness (HV)	Physical properties	
			Density (g/cm <sup>3</sup> )	Porosity(%)
1	1A6Y3S	886.7	3.23	0.11
2	1A6Y3S_M	853.6	3.20	0.14

The analysis of the physical and mechanical properties, as summarized in table 3, shows that the 1A6Y3S frit exhibits the highest bulk density, measured at 3.23 g/cm<sup>3</sup>. In comparison, the 1A6Y3S\_M sample, synthesized via the sol-gel method, displays a slightly lower bulk density of 3.20 g/cm<sup>3</sup>. This reduction is attributed to the predominantly amorphous nature of oxides produced through the sol-gel process, which facilitates lower melting temperatures and improved dispersion of particles.

The data also indicate a trend in porosity, increasing from 0.11% in 1A6Y3S to 0.14% in 1A6Y3S\_M. This inverse relationship between porosity and particle agglomeration can be explained by the degree of densification; higher density typically corresponds to increased compaction, thereby reducing the volume of voids within the material.

Similarly, hardness values follow a trend correlating with density. The 1A6Y3S\_M sample exhibits a Vickers hardness of 853.6 HV, while the 1A6Y3S sample demonstrates a higher hardness of 886.7 HV. This increase in hardness with density is consistent with enhanced structural compactness, which improves the material's resistance to deformation.

These findings suggest that the 1A6Y3S frit, particularly that synthesized through the sol-gel method, possesses superior thermal stability, mechanical integrity, and microstructural uniformity, making it a promising candidate for high-performance ceramic applications.

#### 4. CONCLUSIONS

The 1A6Y3S frit synthesized via the combined sol-gel and co-precipitation method demonstrated superior characteristics compared to the frit produced by conventional solid-state mixing of oxides. This method resulted in a lower phase transition temperature, more controlled phase composition, and improved physical and mechanical properties.

Optimal synthesis conditions for the 1A6Y3S frit were identified as a melting temperature of 1400 °C with a holding time of 5 hours. Under these conditions, the frit exhibited a Vickers hardness of 886.7 HV, a bulk density of 3.23 g/cm<sup>3</sup>, and a low porosity of 0.11%. Thermal analysis indicated that the frit remained fully amorphous up to approximately 1000 °C, with significant crystallization occurring between 1300 and 1400 °C. Above 1300 °C, the predominant crystalline phases formed were Yttrium Disilicate (Y<sub>2</sub>O<sub>3</sub>.2SiO<sub>2</sub>) and Yttrium Silicate (Y<sub>2</sub>O<sub>3</sub>.SiO<sub>2</sub>).

#### REFERENCES

- [1]. TCVN 6530-3:2016: *Vật liệu chịu lửa - Phần 3. Xác định khối lượng thể tích, độ hút nước.*
- [2]. Malinvernì, C., et al., "A yttrium aluminosilicate glass-ceramic to join SiC/SiC composites". Journal of the European Ceramic Society. 44(6): p. 3579-3587, (2024).
- [3]. L. Sun, S. Wang, C. Hou, D. Wang, "Microstructure, mechanical property and bonding mechanism of SiC ceramic joint using a novel Y<sub>2</sub>Si<sub>2</sub>O<sub>7</sub>/Mullite glass-ceramic interlayer". Ceram. Int. 49: p. 17885-17893, (2023).
- [4]. Yang, S., et al., "Effect of CaO doping on the properties and crystallization behavior of Y<sub>2</sub>O<sub>3</sub>-Al<sub>2</sub>O<sub>3</sub>-SiO<sub>2</sub> glass". Ceramics International. 49(20): p. 33188-33196, (2023).
- [5]. J. Denga, B. Lu, K. Hu, J. Wang, "Interaction between Y-Al-Si-O glass-ceramics for environmental barrier coating materials and Ca-Mg-Al-Si-O melts". Ceram. Int. 46: p. 18262-18273, (2022).
- [6]. L. Sun, X. Shi, X. Liu, J. Fang, C. Liu, "Joining of Cf/SiC composites and Si<sub>3</sub>N<sub>4</sub> ceramic with Y<sub>2</sub>O<sub>3</sub>-Al<sub>2</sub>O<sub>3</sub>-SiO<sub>2</sub> glass filler for high-temperature applications". Ceram. Int. 47: p. 15622-15630, (2021).
- [7]. Zheng, Q., et al., "Crystallization behavior and IR structure of yttrium aluminosilicate glasses". Journal of the European Ceramic Society. 40(2): p. 463-471, (2020).
- [8]. Ahmad, S., "Rare-earth Aluminosilicate (RE<sub>2</sub>O<sub>3</sub>-Al<sub>2</sub>O<sub>3</sub>-SiO<sub>2</sub>) Glasses and Their Application as Solders for Joining of Silicon Carbide Components", KIT-Bibliothek, (2018).
- [9]. S. Ahmad et al., "Application of Nd<sub>2</sub>O<sub>3</sub>-Al<sub>2</sub>O<sub>3</sub>-SiO<sub>2</sub> glass solder for joining of silicon carbide components". J. Eur. Ceram. Soc. (2016).
- [10]. L. Gozzelino, V. Casalegno, G. Ghigo, T. Moskalewicz, "He-irradiation effects on glass-ceramics for joining of SiC-based materials". J. Nucl. Mater. 472: p. 28-34, (2016).
- [11]. Yong Li, B. You, W. Zhao, W. Zhang, "Synthesis and Luminescent Properties of Nano-scale Y<sub>2</sub>Si<sub>2</sub>O<sub>7</sub>:Re<sup>3+</sup> (Re=Eu, Tb) Phosphors via Sol-Gel Method". Chinese Journal of Chemical Physics. 21(4):376-380, (2008). DOI:10.1088/1674-0068/21/04/376-380.
- [12]. H. Cinkaya, G. Eryurek, B. D. Bartolo, "White light emission based on both upconversion and thermal processes from Nd<sup>3+</sup> doped yttrium silicate". Ceramics International. 44(4): p. 3541-3547, (2018). <https://doi.org/10.1016/j.ceramint.2017.11.042>.
- [13]. E. Ringdalen, M. Tangstad, "Softening and Melting of SiO<sub>2</sub>, an Important Parameter for Reactions with Quartz in Si Production". Advances in Molten Slags, Fluxes, and Salts: Proceedings of the 10th International Conference on Molten Slags, Fluxes and Salts. p.43-51, (2016). DOI:10.1007/978-3-319-48769-4\_4.

- [14]. C. E. Curtis, "Properties of Yttrium Oxide Ceramics". Journal of the American Ceramic Society. 40(8): p.274 - 278, (2006). DOI:10.1111/j.1151-2916.1957.tb12619.x.

### TÓM TẮT

#### Quá trình hình thành pha khí tổng hợp frit $Al_2O_3 - Y_2O_3 - SiO_2$ bằng phương pháp sol- gel và đồng kết tủa

Frit được ứng dụng nhiều trong ngành công nghiệp do các đặc tính đặc biệt của chúng. Tuy nhiên, hầu hết các frit được chế tạo từ các nguyên liệu là oxit, đòi hỏi nhiệt độ thiêu kết cao và thời gian kéo dài để đạt được độ đồng nhất. Trong nghiên cứu này, quá trình hình thành và phát triển pha khí tổng hợp frit  $Al_2O_3 - Y_2O_3 - SiO_2$  bằng phương pháp sol- gel chỉ cần nhiệt độ tổng hợp thấp và độ tinh khiết cao. Kết quả phổ nhiễu xạ tia X đã xác nhận rằng frit  $Al_2O_3 - Y_2O_3 - SiO_2$  được chế tạo thành công bằng phương pháp sol-gel. Các ảnh hưởng của điều kiện thiêu kết đến quá trình chuyển pha trong vật liệu được nghiên cứu. Các mẫu frit  $Al_2O_3 - Y_2O_3 - SiO_2$  cho thấy cấu trúc hoàn toàn vô định hình ở nhiệt độ gần  $1000^\circ C$ . Theo hàm của nhiệt độ, các pha tinh thể  $Y_2O_3 \cdot 2SiO_2$ ,  $Y_2O_3 \cdot SiO_2$  và  $\alpha-Al_2O_3$  xuất hiện ở khoảng  $1100^\circ C$ ,  $1200^\circ C$  và  $1300^\circ C$ . Pha tinh thể hoàn chỉnh của frit  $Al_2O_3 - Y_2O_3 - SiO_2$  được quan sát thấy ở  $1400^\circ C$ . Các kết quả phân tích nhiệt vi sai xác nhận nhiệt độ chuyển thủy tinh, nhiệt độ đỉnh kết tinh và nhiệt độ eutectic của frit  $Al_2O_3 - Y_2O_3 - SiO_2$ . Bên cạnh đó, điều kiện thiêu kết tối ưu của frit  $Al_2O_3 - Y_2O_3 - SiO_2$  được đề xuất ở  $1400^\circ C$  và 5 giờ.

**Từ khoá:**  $Y_2O_3 - Al_2O_3 - SiO_2$ ; Frit; Gốm kỹ thuật SiALON.